2007

# Thermodynamics of a Statistically Interacting Quantum Gas in *D* Dimensions

Geoffrey G. Potter
*University of Rhode Island*

Gerhard Müller
*University of Rhode Island*, gmuller@uri.edu

***See next page for additional authors***



Citation/Publisher Attribution
Potter, G. G., Müller, G., & Karbach, M. Thermodynamics of statistically interacting quantum gas in D dimensions. *Physical Review E, 76*(6), 061112, 1-12. doi: 10.1103/PhysRevE.76.061112
Available at: http://dx.doi.org/10.1103/PhysRevE.76.061112

# Thermodynamics of a statistically interacting quantum gas in $\mathcal{D}$ dimensions

Geoffrey G. Potter,[1] Gerhard Müller,[1] and Michael Karbach[1,2]
[1]*Department of Physics, University of Rhode Island, Kingston, Rhode Island 02881, USA*
[2]*Fachbereich Mathematik und Naturwissenschaften, Bergische Universität Wuppertal, D-42097 Wuppertal, Germany*
(Received 5 October 2007; published 11 December 2007)

We present the exact thermodynamics (isochores, isotherms, isobars, response functions) of a statistically interacting quantum gas in $\mathcal{D}$ dimensions. The results in $\mathcal{D}=1$ are those of the thermodynamic Bethe ansatz for the nonlinear Schrödinger model, a gas with repulsive two-body contact potential. In all dimensions the ideal boson and fermion gases are recovered in the weak-coupling and strong-coupling limits, respectively. For all nonzero couplings ideal fermion gas behavior emerges for $\mathcal{D}\gg 1$ and, in the limit $\mathcal{D}\to\infty$, a phase transition occurs at $T>0$. Significant deviations from ideal quantum gas behavior are found for intermediate coupling and finite $\mathcal{D}$.

DOI: 10.1103/PhysRevE.76.061112 PACS number(s): 05.30.−d, 75.10.−b

## I. INTRODUCTION

The wave of experimental studies that led to the first observations of Bose-Einstein condensation (BEC) and the development of measurement and confinement technologies have renewed strong interest in the statistical mechanics of interacting quantum gases [1–6]. This line of research can make good use of explicit high-accuracy results from any type of analysis that goes beyond low-density/high-temperature expansions and beyond mean-field theory. Of particular interest are results for response functions, the very quantities most directly amenable to experimental investigations.

Such results can be produced on a rigorous basis for quantum gases with statistical interaction under very general circumstances as shown by Wu [7,8]. The concept of *statistical* interaction introduced by Haldane [9] has proven to be a very useful methodological device to capture the statistical mechanical properties of degrees of freedom subject to *dynamical* interaction. For several model systems in dimension $\mathcal{D}=1$ the coupling between degrees of freedom can be substituted by a generalized Pauli principle with no loss of rigor regarding the thermodynamic analysis [9–13].

Whereas an equivalence between dynamical and statistical interaction is not likely to be realized in $\mathcal{D}>1$ (apart from highly contrived scenarios), models of statistically interacting degrees of freedom can stand on their own. Their thermodynamic properties can be analyzed exactly in any dimension $\mathcal{D}$, producing a full and consistent account of fluctuations as will be demonstrated in this work [14]. The exact results emerging from this analysis make it possible to connect features of the statistical interaction with features of a corresponding dynamical interaction. The systematic study of such connections, in turn, opens the door to the design of (exactly solvable) models of statistical interaction for the description of thermodynamic phenomena associated with specific aspects of dynamical interaction.

In a previous paper [15] we have established a benchmark in that regard by exploring the thermodynamics of an ideal quantum gas with fractional statistics in $\mathcal{D}$ dimensions—a thermodynamic generalization of the Calogero-Sutherland (CS) model [16–18]—taking advantage of techniques and results reported in previous studies [7,8,12,17,19–34]. In that case the statistical interaction was limited to pairs of particles with identical momenta.

Here we relax that constraint and consider a model system, again in $\mathcal{D}$ dimensions, with a statistical interaction that extends to pairs of particles with arbitrary momenta, a system moreover, whose statistical interaction in $\mathcal{D}=1$ is equivalent to the dynamical interaction of a model that is solvable (beyond thermodynamics) via Bethe ansatz: the nonlinear Schrödinger (NLS) model [35–41].

In Sec. II we review the concept of statistical interaction and its use in statistical mechanics. We introduce the NLS model and the generalization of its thermodynamics to $\mathcal{D}>1$. In Sec. III we describe the method of thermodynamic analysis applied to the generalized NLS model. In Sec. IV we discuss selected thermodynamic properties thus calculated. In Sec. V we assess the results in relation to existing benchmarks for ideal quantum gases with fractional statistics.

## II. STATISTICAL INTERACTION

The statistical interaction of any given model system is specified by a generalized Pauli principle [9], expressing how the number of states available to one particle is affected by the presence of other particles.

$$\Delta d_i \doteq -\sum_j g_{ij}\Delta n_j. \tag{1}$$

The indices $i,j$ refer to particle species and the $g_{ij}$ are *statistical interaction coefficients*. For bosons we have $g_{ij}=0$ and for fermions $g_{ij}=\delta_{ij}$. Integrating Eq. (1) yields the holding capacity for particles of species $i$ in the presence of a specific number of particles from each species as follows:

$$d_i = A_i - \sum_j g_{ij}(n_j - \delta_{ij}), \tag{2}$$

where $A_i$ are *statistical capacity constants*. The number of many-particle states composed of $\{n_i\}$ statistically interacting particles is

 

$$W(\{n_i\}) = \prod_i \binom{d_i + n_i - 1}{n_i}. \tag{3}$$

The three principal specifications of a system of particles subject to a statistical interaction are sets of (i) energies $\epsilon_i$, (ii) capacity constants $A_i$, and (iii) interaction coefficients $g_{ij}$. The grand potential of such a system can be expressed in the form [7]

$$\Omega = -k_B T \sum_i A_i \ln\left[\frac{1+w_i}{w_i}\right], \tag{4}$$

where the $w_i$ are determined by the nonlinear algebraic equations,

$$\frac{\epsilon_i - \mu}{k_B T} = \ln(1+w_i) - \sum_j g_{ji} \ln\left(\frac{1+w_j}{w_j}\right). \tag{5}$$

The control variables are $T$ (temperature) and $\mu$ (chemical potential). The average numbers of particles, $\langle n_i \rangle$, are related to the $w_i$ by the linear equations,

$$\sum_j (\delta_{ij} w_j + g_{ij}) \langle n_j \rangle = A_i. \tag{6}$$

If $g_{ij} = g_i \delta_{ij}$ then all Eqs. (5) and (6) are decoupled and the statistical interaction reduces to a (fractional) exclusion condition. This case was the focus of a previous study [15], which includes a simple illustration of the link between combinatorics, Eqs. (1)–(3), and statistical mechanics, Eqs. (4)–(6).

### A. Application to quantum gas

For a nonrelativistic quantum gas in a box of dimensionality $\mathcal{D}$ and volume $V = L^{\mathcal{D}}$ the aforementioned specifications are encoded in the energy-momentum relation $\epsilon_0(k) = |\mathbf{k}|^2$ (in units where $\hbar^2/2m = 1$) and in a function $g(\mathbf{k}, \mathbf{k}')$. The grand potential (4) becomes

$$\Omega = -k_B T \left(\frac{L}{2\pi}\right)^{\mathcal{D}} \int d^{\mathcal{D}}k \ln \frac{1+w_{\mathbf{k}}}{w_{\mathbf{k}}}, \tag{7}$$

where $w_{\mathbf{k}}$ is the solution of the nonlinear integral equation

$$\frac{|\mathbf{k}|^2 - \mu}{k_B T} = \ln(1+w_{\mathbf{k}}) - \int d^{\mathcal{D}}k' g(\mathbf{k}', \mathbf{k}) \ln \frac{1+w_{\mathbf{k}'}}{w_{\mathbf{k}'}}. \tag{8}$$

The particle density in $\mathbf{k}$ space, $\langle n_{\mathbf{k}} \rangle$, is the solution of the linear integral equation

$$\langle n_{\mathbf{k}} \rangle w_{\mathbf{k}} + \int d^{\mathcal{D}}k' g(\mathbf{k}, \mathbf{k}') \langle n_{\mathbf{k}'} \rangle = 1. \tag{9}$$

The fundamental thermodynamic relations (thermodynamic and caloric equations of state) depend on the solutions of Eqs. (8) and (9) as follows:

$$\frac{pV}{k_B T} = \left(\frac{L}{2\pi}\right)^{\mathcal{D}} \int d^{\mathcal{D}}k \ln \frac{1+w_{\mathbf{k}}}{w_{\mathbf{k}}}, \tag{10}$$

$$\mathcal{N} = \left(\frac{L}{2\pi}\right)^{\mathcal{D}} \int d^{\mathcal{D}}k \langle n_{\mathbf{k}} \rangle, \tag{11}$$

$$U = \left(\frac{L}{2\pi}\right)^{\mathcal{D}} \int d^{\mathcal{D}}k |\mathbf{k}|^2 \langle n_{\mathbf{k}} \rangle. \tag{12}$$

If the statistical interaction is of the form $g(|\mathbf{k} - \mathbf{k}'|)$ then the solutions of Eqs. (8) and (9) only depend on the magnitude of the particle momenta.

### B. Nonlinear Schrödinger model

Consider the boson gas in $\mathcal{D} = 1$ with a repulsive contact interaction of strength $c$ as described by the NLS Hamiltonian

$$H = -\sum_{i=1}^{N} \frac{\partial^2}{\partial x_i^2} + 2c \sum_{j<i} \delta(x_i - x_j). \tag{13}$$

The thermodynamic Bethe ansatz (TBA) solution [37–40] of the NLS model expresses the grand potential in the form

$$\Omega(T, L, \mu) = -k_B T \left(\frac{L}{2\pi}\right) \int_{-\infty}^{+\infty} dk \ln(1 + e^{-\epsilon(k)/k_B T}), \tag{14}$$

where $\epsilon(k)$ is the solution of the Yang-Yang equation [37],

$$\epsilon(k) = k^2 - \mu - \frac{k_B T}{2\pi} \int_{-\infty}^{+\infty} dk' K(k - k') \ln(1 + e^{-\epsilon(k')/k_B T}), \tag{15}$$

with kernel

$$K(k - k') = \frac{2c}{c^2 + (k - k')^2}. \tag{16}$$

The particle density $\langle n_k \rangle$ is the solution, for given $\epsilon(k)$, of the Lieb-Liniger equation [35,37],

$$\langle n_k \rangle [1 + e^{\epsilon(k)/k_B T}] = 1 + \frac{1}{2\pi} \int_{-\infty}^{+\infty} dk' K(k - k') \langle n_{k'} \rangle. \tag{17}$$

Bernard and Wu [12] showed that this TBA solution is equivalent to the thermodynamics of a statistically interacting gas in $\mathcal{D} = 1$ if the following identifications are made:

$$w_k = e^{\epsilon(k)/k_B T}, \tag{18a}$$

$$g(k - k') = \delta(k - k') - \frac{1}{2\pi} K(k - k'). \tag{18b}$$

### C. Generalization of NLS model

The generalized NLS model is a quantum gas in $\mathcal{D}$ dimensions with the statistical interaction expressed by the kernel

$$K(\mathbf{k} - \mathbf{k}') = \frac{2\Gamma(\mathcal{D})}{\pi^{\mathcal{D}/2 - 1} \Gamma(\mathcal{D}/2)} \frac{c^{\mathcal{D}}}{[c^2 + (\mathbf{k} - \mathbf{k}')^2]^{\mathcal{D}}} \tag{19}$$

of the Yang-Yang equation (15) and Lieb-Liniger equation (17) generalized to $\mathcal{D} \geqslant 1$ and designed to reproduce the exact thermodynamics of the dynamically interacting NLS model in $\mathcal{D} = 1$. The kernel (19) has the properties

$$\lim_{c\to\infty} K(\mathbf{k}) = 0, \tag{20a}$$

$$\lim_{c\to 0} K(\mathbf{k}) = 2\pi\delta(\mathbf{k}), \tag{20b}$$

$$\int d^{\mathcal{D}}k K(\mathbf{k}) = 2\pi. \tag{20c}$$

This model interpolates between the ideal Fermi-Dirac (FD) gas in the strong-coupling limit ($c=\infty$) and the ideal Bose-Einstein (BE) gas in the weak-coupling limit ($c=0$) in all dimensions $\mathcal{D}\geqslant 1$. In the limit $\mathcal{D}\to\infty$ it turns into the ideal FD gas for all $c>0$.

For the further analysis of the generalized NLS model we reduce Eqs. (8) and (9) into integral equations for the functions

$$\epsilon(k) \doteq k_B T \ln w_{\mathbf{k}}, \quad n(k) \doteq \langle n_{\mathbf{k}} \rangle, \tag{21}$$

where $k \doteq |\mathbf{k}|$. We also introduce scaled quantities

$$\bar{k} \doteq \frac{k}{\sqrt{k_B T}}, \quad \bar{c} \doteq \frac{c}{\sqrt{k_B T}}, \tag{22a}$$

$$\bar{\epsilon}(\bar{k}) \doteq \frac{\epsilon(k)}{k_B T}, \quad \bar{n}(\bar{k}) \doteq n(k). \tag{22b}$$

Equations (15) and (17) thus thermodynamically generalized to $\mathcal{D}\geqslant 1$ become

$$\bar{\epsilon}(\bar{k}) = \bar{k}^2 - \ln z - \int_0^\infty d\bar{k}' \bar{K}(\bar{k},\bar{k}') \ln(1 + e^{-\bar{\epsilon}(\bar{k}')}), \tag{23}$$

$$\bar{n}(\bar{k})[1 + e^{\bar{\epsilon}(\bar{k})}] = 1 + \int_0^\infty d\bar{k}' \bar{K}(\bar{k},\bar{k}') \bar{n}(\bar{k}'), \tag{24}$$

with fugacity $z=e^{\mu/k_B T}$ and reduced kernel

$$\bar{K}(\bar{k},\bar{k}') = \frac{2\bar{c}^{\mathcal{D}}\Gamma(\mathcal{D})}{[\Gamma(\mathcal{D}/2)]^2} \times \frac{\bar{k}'^{\mathcal{D}-1}(\bar{c}^2 + \bar{k}^2 + \bar{k}'^2)}{[\bar{c}^4 + 2\bar{c}^2(\bar{k}^2 + \bar{k}'^2) + (\bar{k}^2 - \bar{k}'^2)^2]^{(\mathcal{D}+1)/2}}. \tag{25}$$

Any particular solution $\bar{\epsilon}(\bar{k}), \bar{n}(\bar{k})$ at fixed $z, \bar{c}$ describes the system over a range of temperature $T$, chemical potential $\mu$, and coupling constant $c$. For couplings $0<\bar{c}<\infty$ the solutions of Eqs. (23) and (24) also depend on $\mathcal{D}$. High-precision data for $\bar{\epsilon}(\bar{k}), \bar{n}(\bar{k})$ can be obtained from an iterative solution. The sample of data shown in Fig. 1 exhibit the main characteristic features of these functions.

The function $\bar{\epsilon}(\bar{k}) + \ln z$ is monotonically increasing from a minimum at $\bar{k}=0$. The dependence on $z$, $\bar{c}$ (not shown), and $\mathcal{D}$ is strongest at small $\bar{k}$ and weakens rapidly at $\bar{k}>1$. The presence of a shoulder combined with a deep minimum at $\bar{k}=0$ signals a BEC ordering tendency (weakly evident here in the $\mathcal{D}>2$ data). The function $\bar{n}(\bar{k})$ is monotonically decreasing from a maximum at $\bar{k}=0$. Again there is a significant dependence on $z$, $\bar{c}$, and $\mathcal{D}$ at small $\bar{k}$. The function itself vanishes rapidly at $\bar{k}>1$.

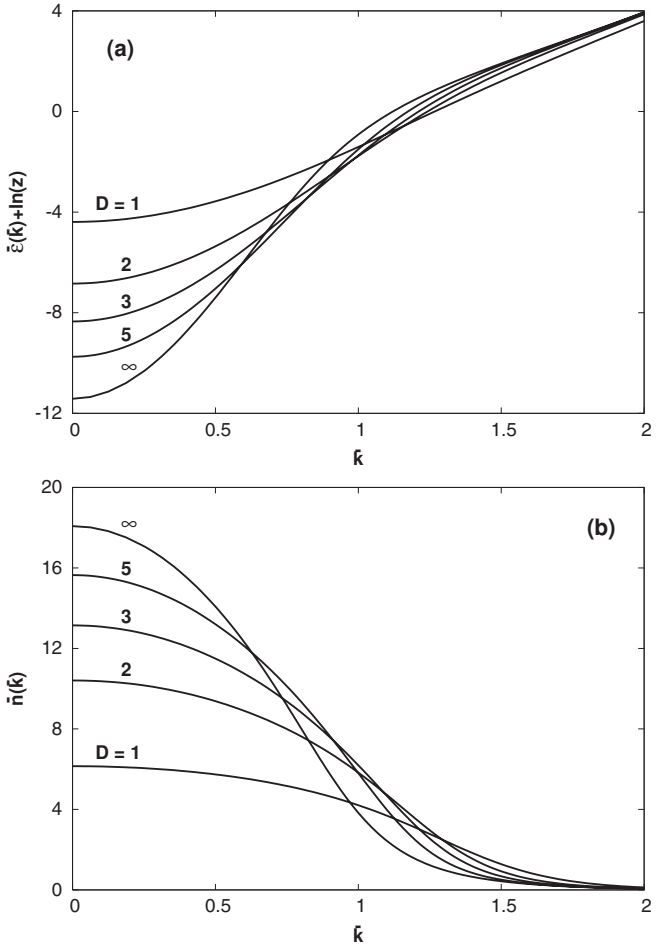


FIG. 1. Iterative solutions (a) $\bar{\epsilon}(\bar{k}) + \ln z$ of Eq. (23), and (b) $\bar{n}(\bar{k})$ of Eq. (24) for $\bar{c}=0.25$, $z=3$, and various values of $\mathcal{D}$. The curves for $\mathcal{D}=\infty$ are solutions of Eqs. (29) and (30).

The dependence on $k, \mu, T$ of the functions $\bar{\epsilon}(\bar{k})$ and $\bar{n}(\bar{k})$ is not reducible, for $0<\bar{c}<\infty$, to a dependence on a single variable, $(k^2-\mu)/k_B T$. This represents a major deviation from a signature property of ideal gases.

### D. Limiting cases

In the strong-coupling and weak-coupling limits, which are fixed points of the scaling relation for the coupling constant, we recover the familiar FD and BE results as follows:

$$\bar{\epsilon}(\bar{k}) = \bar{k}^2 - \ln z, \quad \bar{n}(\bar{k}) = \left(\frac{1}{z}e^{\bar{k}^2} + 1\right)^{-1}, \tag{26}$$

for $\bar{c}=\infty$, and

$$\bar{\epsilon}(\bar{k}) = \ln\left(\frac{1}{z}e^{\bar{k}^2} - 1\right), \quad \bar{n}(\bar{k}) = \left(\frac{1}{z}e^{\bar{k}^2} - 1\right)^{-1} \tag{27}$$

for $\bar{c}=0$. The $\mathcal{D}$ independence of these functions is another signature property of ideal gases, a property upheld in the presence of fractional statistics [15]. The parabolic curve, $\bar{\epsilon}(\bar{k})+\ln z=\bar{k}^2$, may serve as the baseline for the solutions of Eq. (23). It is exact in the strong-coupling limit for all $z>0$, but only for $z\to 0$ in the weak-coupling limit. For $0<z<1$ the deviations of $\bar{\epsilon}(\bar{k})+\ln z$ from $\bar{k}^2$ and of $\bar{n}(\bar{k})$ from zero are suppressed by factors $\sim e^{-\bar{k}^2}$ as $\bar{k}$ increases. We have noted very similar behavior in the numerical results for $0<c<\infty$.

In the limit $\mathcal{D}\to\infty$ the reduced kernel (25) acquires a much simpler structure,

$$\lim_{\mathcal{D}\to\infty} \bar{K}(\bar{k},\bar{k}') = \delta(\bar{k}' - \sqrt{\bar{k}^2+\bar{c}^2}), \tag{28}$$

but the $\bar{c}$ dependence is retained and (for $\bar{c}>0$) also the statistical coupling of particles with distinct momenta. Equations (23) and (24), with reduced kernel (28) turn into the implicit functions

$$\bar{\epsilon}(\bar{k}) = \bar{k}^2 - \ln z - \ln(1+e^{-\bar{\epsilon}(\sqrt{\bar{k}^2+\bar{c}^2})}), \tag{29}$$

$$\bar{n}(\bar{k})[1+e^{\bar{\epsilon}(\bar{k})}] = 1+\bar{n}(\sqrt{\bar{k}^2+\bar{c}^2}). \tag{30}$$

The solution of Eq. (29) is

$$e^{-\bar{\epsilon}(\bar{k})} = \sum_{l=0}^{\infty} z^{l+1} e^{-(l+1)\bar{k}^2} e^{-\bar{c}^2 l(l+1)/2}, \tag{31}$$

and the solution of Eq. (30) is

$$\bar{n}(\bar{k}) = \sum_{l=0}^{\infty} \alpha_l z^{l+1} e^{-\bar{k}^2(l+1)}, \tag{32}$$

with the recursion

$$\alpha_l = e^{-(\bar{c}^2/2)l(l+1)} - \sum_{j=1}^{l} (\alpha_{l-j} e^{-(\bar{c}^2/2)j(j-1)} - \alpha_{j-1} e^{-(\bar{c}^2/2)[(l-j)(l-j+1)+2j]}). \tag{33}$$

For $\bar{c}\to\infty$ Eqs. (26) are recovered, and for $\bar{c}\to 0$ Eqs. (27) are recovered.

## III. THERMODYNAMIC ANALYSIS OF GENERALIZED NLS MODEL

Exact results for the thermodynamics of the generalized NLS model in $\mathcal{D}\geqslant 1$ and across the range $0\leqslant c\leqslant\infty$ of coupling strengths can now be calculated from the solutions $\bar{\epsilon}(\bar{k})$ and $\bar{n}(\bar{k})$ of Eqs. (23) and (24), respectively.

### A. NLS functions

The fundamental thermodynamic relations (10)–(12) are rewritten in the form

$$\frac{p\lambda_T^{\mathcal{D}}}{k_B T} = F_p^{(\mathcal{D})}(z,\bar{c}), \tag{34}$$

$$\frac{\mathcal{N}\lambda_T^{\mathcal{D}}}{V} = F_{\mathcal{N}}^{(\mathcal{D})}(z,\bar{c})\left[+\frac{z}{1-z}\right], \tag{35}$$

$$\frac{U\lambda_T^{\mathcal{D}}}{V}\Big/\frac{\mathcal{D}}{2}k_B T = F_U^{(\mathcal{D})}(z,\bar{c}), \tag{36}$$

where

$$\lambda_T \doteq \sqrt{\frac{h^2}{2\pi m k_B T}} \overset{\hbar^2/2m=1}{\to} \sqrt{\frac{4\pi}{k_B T}} \tag{37}$$

is the thermal wavelength and the term in Eq. (35) enclosed by square brackets is relevant only if $\bar{c}=0$ and $\mathcal{D}>2$. The NLS functions in Eqs. (34)–(36) are defined as follows:

$$F_p^{(\mathcal{D})}(z,\bar{c}) \doteq \frac{2}{\Gamma(\mathcal{D}/2)}\int_0^{\infty} d\bar{k}\bar{k}^{\mathcal{D}-1}\ln(1+e^{-\bar{\epsilon}(\bar{k})}), \tag{38}$$

$$F_{\mathcal{N}}^{(\mathcal{D})}(z,\bar{c}) \doteq \frac{2}{\Gamma(\mathcal{D}/2)}\int_0^{\infty} d\bar{k}\bar{k}^{\mathcal{D}-1}\bar{n}(\bar{k}), \tag{39}$$

$$F_U^{(\mathcal{D})}(z,\bar{c}) \doteq \frac{2}{\Gamma(\mathcal{D}/2+1)}\int_0^{\infty} d\bar{k}\bar{k}^{\mathcal{D}+1}\bar{n}(\bar{k}), \tag{40}$$

where the additional dependence of $\bar{\epsilon}(\bar{k}),\bar{n}(\bar{k})$ on $\mathcal{D}$, $\bar{c}$, $z$ is implied.

In the strong-coupling and weak-coupling limits, the NLS functions turn into the familiar FD functions,

$$f_n(z) \doteq \frac{1}{\Gamma(n)}\int_0^{\infty}\frac{dx x^{n-1}}{z^{-1}e^x+1}, \quad z\geqslant 0, \tag{41}$$

and BE functions,

$$g_n(z) \doteq \frac{1}{\Gamma(n)}\int_0^{\infty}\frac{dx x^{n-1}}{z^{-1}e^x-1}, \quad 0\leqslant z\leqslant 1, \tag{42}$$

respectively,

$$F_p^{(\mathcal{D})}(z,\infty) = F_U^{(\mathcal{D})}(z,\infty) = f_{\mathcal{D}/2+1}(z), \tag{43a}$$

$$F_{\mathcal{N}}^{(\mathcal{D})}(z,\infty) = f_{\mathcal{D}/2}(z), \tag{43b}$$

and

$$F_p^{(\mathcal{D})}(z,0) = F_U^{(\mathcal{D})}(z,0) = g_{\mathcal{D}/2+1}(z), \tag{44a}$$

$$F_{\mathcal{N}}^{(\mathcal{D})}(z,0) = g_{\mathcal{D}/2}(z). \tag{44b}$$

Furthermore, for $\mathcal{D}\gg 1$ fermionic behavior results for any $\bar{c}>0$ as follows:

$$F_p^{(\mathcal{D})}(z,\bar{c}), F_U^{(\mathcal{D})}(z,\bar{c}) \overset{\mathcal{D}\gg 1}{\rightsquigarrow} f_{\mathcal{D}/2+1}(z), \tag{45a}$$

$$F_{\mathcal{N}}^{(\mathcal{D})}(z,\bar{c}) \overset{\mathcal{D}\gg 1}{\rightsquigarrow} f_{\mathcal{D}/2}(z). \tag{45b}$$

With increasing $\mathcal{D}$ the factor $\bar{k}^{\mathcal{D}\pm 1}$ pushes all significant contributions to the integrals (38)–(40) toward larger and larger $\bar{k}$, where the deviations of $\bar{\epsilon}(\bar{k})$ and $\bar{n}(\bar{k})$ from their ($\bar{c}=\infty$)

values (26) become smaller and smaller [42].

A characteristic ideal-gas property is that the dependence of the fugacity on the thermodynamic variables $T,V,\mathcal{N}$ is expressible as a function of a single variable,

$$x \doteq \lambda_T v^{-1/\mathcal{D}}, \quad v \doteq V/\mathcal{N}. \tag{46}$$

In the Maxwell-Boltzmann (MB) gas we have $x^{\mathcal{D}}=z$, in the FD gas $x^{\mathcal{D}}=f_{\mathcal{D}/2}(z)$, and in the BE gas $x^{\mathcal{D}}=g_{\mathcal{D}/2}(z)$. A unique functional relation persists in the case of fractional statistics [15]. In the generalized NLS model, however, we have $x^{\mathcal{D}}=F_{\mathcal{N}}^{(\mathcal{D})}(z,\bar{c})$ with a separate $T$ dependence contained in $\bar{c}$. For ideal quantum gases, including those with fractional statistics, there also exists a unique functional dependence of $pV/\mathcal{N}k_BT$ on $z$. Again this no longer holds in the generalized NLS model, where we have $pV/\mathcal{N}k_BT=F_p^{(\mathcal{D})}(z,\bar{c})/F_{\mathcal{N}}^{(\mathcal{D})}(z,\bar{c})$.

### B. Reference values

We introduce reference values for the thermodynamic variables $v,T,p$ based on the thermal wavelength $\lambda_T$ and the MB equation of state $pv=k_BT$ in the presentation of our data below.

$$k_BT_v = \frac{4\pi}{v^{2/\mathcal{D}}}, \quad p_v = \frac{4\pi}{v^{2/\mathcal{D}+1}} \quad (v=\text{const}), \tag{47}$$

$$v_T = \left(\frac{4\pi}{k_BT}\right)^{\mathcal{D}/2}, \quad p_T = \frac{(k_BT)^{\mathcal{D}/2+1}}{(4\pi)^{\mathcal{D}/2}} \quad (T=\text{const}), \tag{48}$$

$$k_BT_p = 4\pi\left(\frac{p}{4\pi}\right)^{2/(\mathcal{D}+2)}, \quad v_p = \left(\frac{4\pi}{p}\right)^{\mathcal{D}/(\mathcal{D}+2)} \quad (p=\text{const}). \tag{49}$$

They are especially useful in comparative plots that encompass the full range of $\bar{c}$ at finite $\mathcal{D}$.

For the thermodynamic analysis we must adapt the NLS functions to the type of process under consideration. Each function has a different $z$ dependence at fixed $c$, depending, for example, on whether we consider $v=$const, $T=$const, or $p=$const. To this end we introduce three kinds of reduced coupling constants for use in isochoric, isothermal, and isobaric processes, respectively,

$$c_v \doteq \frac{c}{\sqrt{k_BT_v}} = \bar{c}\sqrt{\frac{T}{T_v}} = \frac{\bar{c}}{x} \quad (v=\text{const}), \tag{50}$$

$$c_T \doteq \frac{c}{\sqrt{k_BT}} = \bar{c} \quad (T=\text{const}), \tag{51}$$

$$c_p \doteq \frac{c}{\sqrt{k_BT_p}} = \bar{c}\sqrt{\frac{T}{T_p}} \doteq \frac{\bar{c}}{y} \quad (p=\text{const}), \tag{52}$$

where $x$ and $y$ are the solutions of

$$x^{\mathcal{D}} = F_{\mathcal{N}}^{(\mathcal{D})}(z,c_vx), \tag{53}$$

$$y^{\mathcal{D}+2} = F_p^{(\mathcal{D})}(z,c_py), \tag{54}$$

respectively.

Reference values based on the chemical potential of the FD gas present themselves as an alternative in some situations. Defining $\ln z \doteq \bar{T}_v/T$ in isochoric processes and $\ln z \doteq \bar{T}_p/T$ in isobaric processes, we have

$$\frac{\bar{T}_v}{T_v} = \frac{\bar{p}_v}{p_v} = \left[\Gamma\left(\frac{\mathcal{D}}{2}+1\right)\right]^{2/\mathcal{D}} \overset{\mathcal{D}\gg 1}{\rightsquigarrow} \frac{\mathcal{D}}{2e} \tag{55}$$

for $v=$const, and

$$\frac{\bar{T}_p}{T_p} = \frac{\bar{v}_p}{v_p} = \left[\Gamma\left(\frac{\mathcal{D}}{2}+2\right)\right]^{2/(\mathcal{D}+2)} \overset{\mathcal{D}\gg 1}{\rightsquigarrow} \left(\frac{\mathcal{D}}{2}+1\right)\frac{1}{e} \tag{56}$$

for $p=$const. The divergence of these ratios in the limit $\mathcal{D}\to\infty$ has some surprising consequence as will be discussed in Sec. IV B.

## IV. RESULTS

In Ref. [15] we presented a panoramic view of the thermodynamics of the generalized CS model (ideal quantum gas with fractional statistics) in $\mathcal{D}$ dimensions. The emphasis was on the crossover between bosonlike and fermionlike features in isochores, isotherms, isobars, response functions, and the speed of sound as caused by aspects of the statistical interaction that reflect long-range attraction and short-range repulsion.

The generalized NLS model considered here exhibits some similarities with the generalized CS model regarding thermodynamic properties, especially their dependence on the coupling constants of the two models. However, there are notable differences, many of which can be identified as significant deviations from ideal gas behavior. In our presentation of results we highlight these deviations and the role of dimensionality.

### A. Isochores, isobars, and isotherms

The dependences of $p$ on $T$ at $v=$const, of $v$ on $T$ at $p=$const, and of $p$ on $v$ at $T=$const are determined by Eqs. (34) and (35) in parametric representations,

$$\frac{p}{p_v} = \frac{F_p^{(\mathcal{D})}(z,c_vx)}{[F_{\mathcal{N}}^{(\mathcal{D})}(z,c_vx)]^{1+2/\mathcal{D}}}, \quad \frac{T}{T_v} = [F_{\mathcal{N}}^{(\mathcal{D})}(z,c_vx)]^{-2/\mathcal{D}}, \tag{57}$$

$$\frac{v}{v_p} = \frac{[F_p^{(\mathcal{D})}(z,c_py)]^{\mathcal{D}/(\mathcal{D}+2)}}{F_{\mathcal{N}}^{(\mathcal{D})}(z,c_py)}, \quad \frac{T}{T_p} = [F_p^{(\mathcal{D})}(z,c_py)]^{-2/(\mathcal{D}+2)}, \tag{58}$$

$$\frac{p}{p_T} = F_p^{(\mathcal{D})}(z,c_T), \quad \frac{v}{v_T} = [F_{\mathcal{N}}^{(\mathcal{D})}(z,c_T)]^{-1}, \tag{59}$$

respectively, with the fugacity $z$ in the role of the parameter. Here $x$ and $y$ are the solutions of Eqs. (53) and (54), respectively.

In Fig. 2 we show isochores, isobars, and isotherms for various coupling strengths $c_{v,p,T}$ in $\mathcal{D}=3$. The variation of the curves between the (weak-coupling) boson limit and the

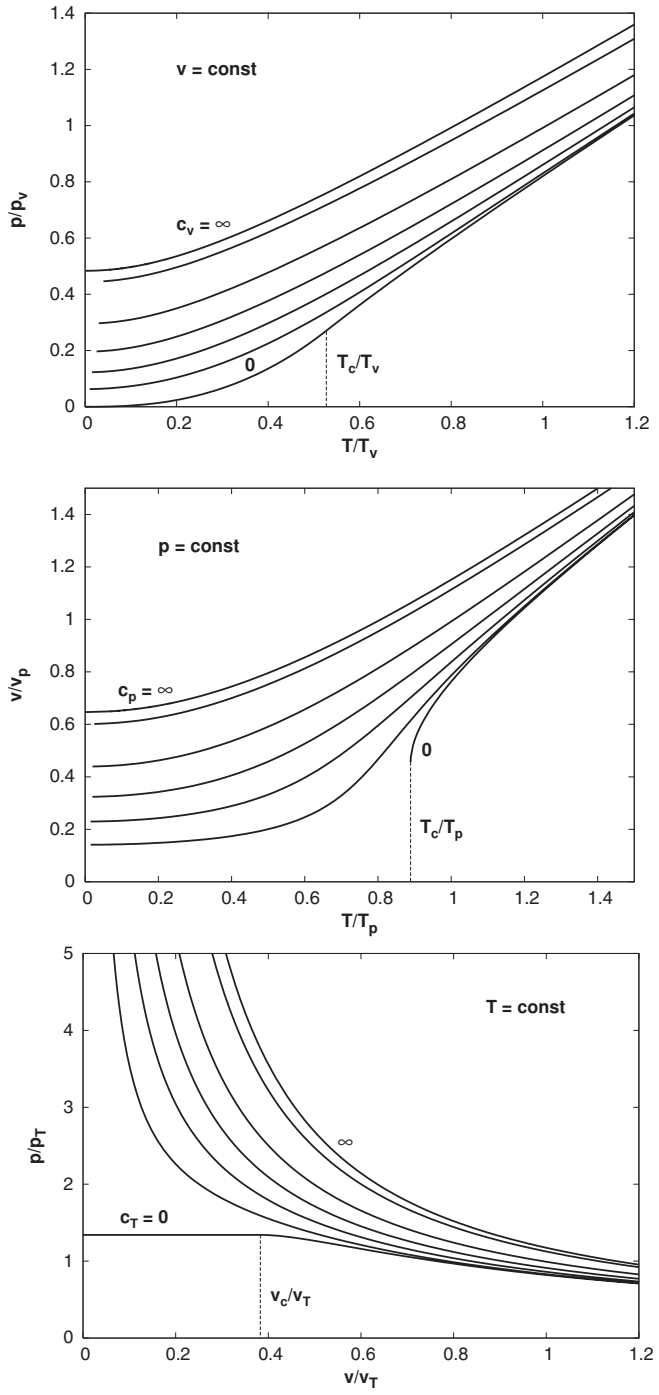


FIG. 2. Isochores, isobars, and isotherms in $D=3$ for $c_{v,p,T}=0$, 0.1, 0.25, 0.5, 1, 3, $\infty$ (from the bottom up in each frame).

(strong-coupling) fermion limit is similar to what was observed in the generalized CS model [15]: the convergence of all curves toward the MB line at high $T$ or large $v$, and the fanning out at low $T$ or small $v$. Corresponding plots in other $\mathcal{D}$ show similar trends in the two models.

The shape of the curves for $c_{v,p,T}>0$ in Fig. 2 yield some insight into the physical interpretation of the statistical interaction. For weak couplings ($c_{v,p,T}<1$) the curves exhibit bosonlike features at high $T$ or large $v$ and fermionlike features at low $T$ or small $v$. These observations translate into a long-range attractive part and a shorter-range repulsive part of the statistical interaction. The attractive tail is only present for small $c_{v,p,T}$, whereas the repulsive core is conspicuous for all $c_{v,p,T}>0$.

Among all the curves only the ones pertaining to the boson limit ($c_{v,p,T}=0$) have a singularity. This singularity signals the presence of a phase transition, the onset of BEC. In the $\mathcal{D}=3$ case shown, the phase transition occurs at $T_c/T_v \simeq 0.527$, $p_c/p_v \simeq 0.271$ along the isochore, at $T_c/T_p \simeq 0.889$, $v_c/v_p \simeq 0.456$ along the isobar, and at $v_c/v_T \simeq 0.383$, $p_c/p_T \simeq 1.341$ along the isotherm.

The bosonic isochore has a singularity at $T_c/T_v>0$ only in $\mathcal{D}>2$. In $2<\mathcal{D}\leqslant 4$ it has a discontinuity in curvature. In $\mathcal{D}>4$ it becomes a discontinuity in slope. In the limit $\mathcal{D}\to\infty$ the bosonic isochore itself becomes discontinuous. By contrast, the bosonic isobar has a singularity at $T_c/T_p>0$ in all dimensions $\mathcal{D}\geqslant 1$, but with $v_c/v_p>0$ only in $\mathcal{D}>2$. The bosonic isotherm has a horizontal portion at $v/v_T<v_c/v_T$ in $\mathcal{D}>2$ (see Ref. [15] for more details on the bosonic curves.)

We have already noted that all three NLS functions (38)–(40) converge toward the corresponding FD functions as $\mathcal{D}\to\infty$ provided we have $\bar{c}>0$. One reflection of this fact in the data for isochores, isobars, and isotherms is that all curves for $c_{v,p,T}>0$ move closer together as $\mathcal{D}$ increases. They coalesce into the universal curve (isochore, isobar, or isotherm) representing the ideal FD gas in $\mathcal{D}=\infty$. Only the bosonic curves at $T<T_c$ or $v<v_c$ stay apart.

In Fig. 3 we show two sets of isochores, isobars, and isotherms for the generalized NLS model in $\mathcal{D}=1,2,3$, one set for weak coupling, the other for strong coupling. Also shown (dashed) are the corresponding curves pertaining to $\mathcal{D}=\infty$, which will be derived in Sec. IV B. For the most part, the weak-coupling and strong-coupling curves are located on opposite sides of the dashed line in each frame.

Convergence of the data for $\mathcal{D}=1,2,3$ toward the line representing $\mathcal{D}=\infty$ is only apparent at high $T$ or large $v$ and more clearly in the strong-coupling data than in the weak-coupling data. This is not surprising in view of the observation made earlier in the context of Fig. 2 that for weak couplings the (effectively) long-range attractive part and short-range repulsive part of the statistical interaction are responsible for opposing trends and a crossover between them. However, convergence becomes manifest in higher $\mathcal{D}$ (not shown) as the NLS functions gradually turn into FD functions first for strong couplings and then also for weak couplings.

### B. Phase transition in $\mathcal{D}=\infty$

It is well known that no phase transition at $T>0$ exists for free fermions in $\mathcal{D}<\infty$. No transition is expected to exist in the generalized NLS model in finite $\mathcal{D}$ except in the boson limit. However, a curious transition does emerge in the limit $\mathcal{D}\to\infty$, where the generalized NLS model with $\bar{c}>0$ effectively turns into an ideal FD gas.

To determine the thermodynamic equation of state, $f(p,v,T)=0$, of the generalized NLS model in $\mathcal{D}=\infty$ we recall Eq. (45) and rewrite Eqs. (57)–(59) for $\mathcal{D}\gg 1$ with the FD functions substituted for the NLS functions. A singularity

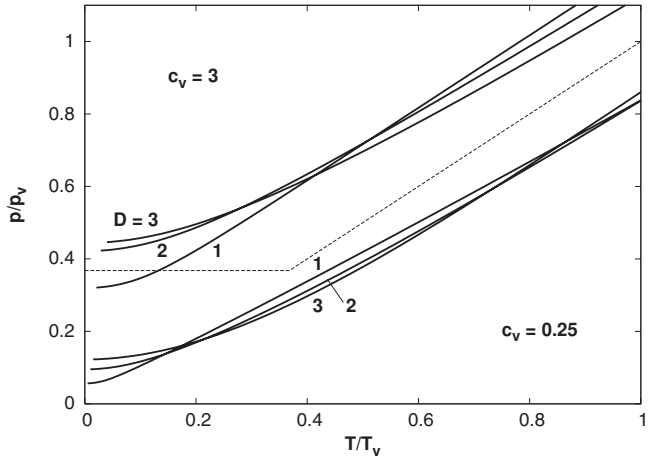


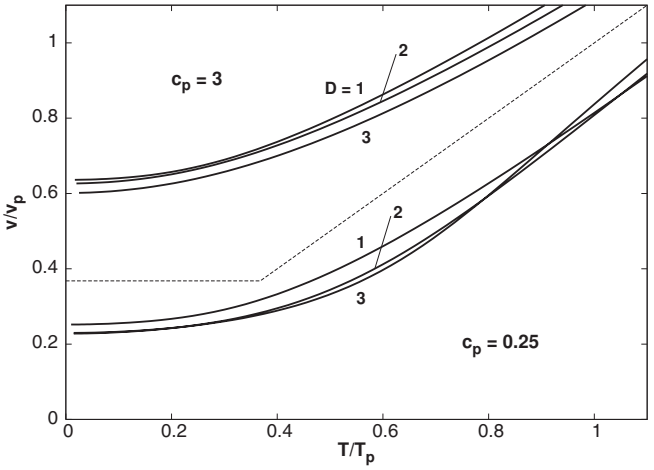


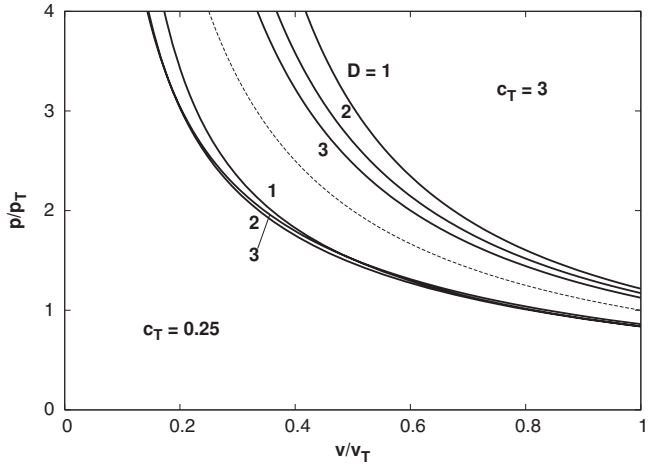


FIG. 3. Isochores, isobars, and isotherms in $D=1,2,3$ for $c_{v,p,T}=0.25$ and $c_{v,p,T}=3$. The dashed lines represent the curves for $\mathcal{D}=\infty$.

at $T>0$ results as a consequence of the fact that the two limits $\mathcal{D}\to\infty$, $z\to\infty$ are not interchangeable. The emergence of the singularity is apparent in the isochores and isobars in $\mathcal{D}\gg 1$ as shown in Fig. 4.

The isochore at $z<\infty$ in the limit $\mathcal{D}\to\infty$ yields a straight-line segment with unit slope and zero intercept in the $(T/T_v, p/p_v)$ plane over a nonzero interval $T_c\leqslant T\leqslant\infty$ as follows:

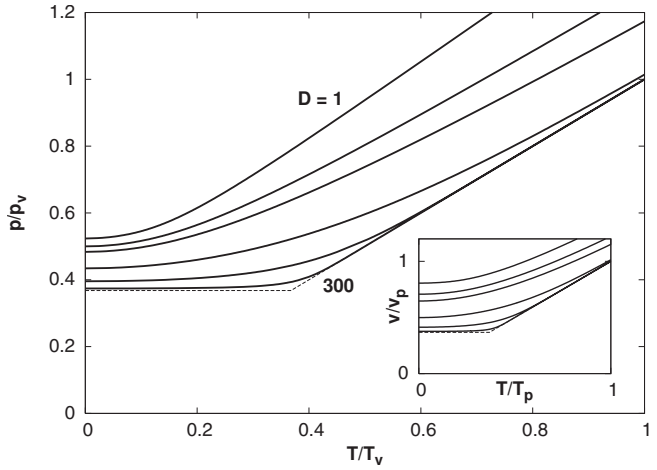


FIG. 4. Isochores (main plot) and isobars (inset) of the ideal FD gas in $\mathcal{D}=1,2,3,10,40,300$ (top to bottom). The result for $\mathcal{D}=\infty$ is represented by the dashed lines.

$$\frac{p}{p_v}\overset{\mathcal{D}\gg 1}{\simeq}\frac{T}{T_v}\frac{f_{\mathcal{D}/2+1}(z)}{f_{\mathcal{D}/2}(z)}\overset{\mathcal{D}\to\infty}{\to}\frac{T}{T_v}. \tag{60}$$

The reference values (47) become $k_BT_v=4\pi$, $p_v=4\pi/v$ in the limit $\mathcal{D}\to\infty$. The same isochore in the limit $\mathcal{D}\to\infty$, $z\to\infty$ with $\mathcal{D}/2=r\ln z$, $r\geqslant 0$ yields a horizontal line segment over a nonzero interval $0\leqslant T\leqslant T_c$ as follows:

$$\frac{p}{p_v}\overset{\mathcal{D}\gg 1}{\simeq}\frac{f_{\mathcal{D}/2+1}(z)}{[f_{\mathcal{D}/2}(z)]^{1+2/\mathcal{D}}}\overset{z\gg 1}{\rightsquigarrow}\frac{e^{-1}}{1+2/\mathcal{D}}, \tag{61}$$

$$\frac{T}{T_v}\overset{\mathcal{D}\gg 1}{\simeq}[f_{\mathcal{D}/2}(z)]^{-2/\mathcal{D}}\overset{z\gg 1}{\rightsquigarrow}\frac{\mathcal{D}}{2}\frac{e^{-1}}{\ln z}, \tag{62}$$

where we have used the leading term in the asymptotic expansion of the FD function [43]. The value of $T_c$ is determined by the intersection point of the two line segments. The equation of state thus reads [44]

$$pv=\begin{cases}k_BT, & T>T_c\\ k_BT_c, & T<T_c,\end{cases}\qquad k_BT_c=\frac{4\pi}{e}. \tag{63}$$

This same universal relation can also be inferred from Eq. (58) for the isobar or from Eq. (59) for the isotherm by performing the appropriate limits. All isotherms are hyperbolas, including the transition line at $T=T_c$. All the isochores and isobars consist of two straight-line segments with the singularity at $T=T_c$ as already shown in Fig. 4.

This somewhat unusual phase transition from a fully intact Fermi sea at $T<T_c$ to an ideal MB gas at $T>T_c$ results from the conspiracy of two opposing effects, one suppressing thermal excitations at low $T$ and the other enhancing them at high $T$. Both effects grow stronger in higher dimensions.

We know from Eq. (55) that as $\mathcal{D}$ increases the reference temperature $T_v$ becomes smaller and smaller compared to the Fermi temperature $\bar{T}_v$ in isochoric processes (considered here for specificity). This suppresses any rise in pressure at sufficiently small but nonzero $T/T_v$ more and more strongly. In

the limit $\mathcal{D}\to\infty$, as $T_v/\bar{T}_v\to 0$, the pressure will remain constant over a nonvanishing interval of $T/T_v$ at the value $p/p_v=e^{-1}$ exerted by the perfect Fermi sea.

We also know (e.g., from analogies to microcanonical ensembles) that as $\mathcal{D}$ increases the energy density of one-particle states is progressively thinned out inside the surface of the Fermi hypersphere except close to the surface. The consequence is that a smaller and smaller amount of thermal energy is needed to knock out the vast majority of particles from the Fermi sea. Moreover, the density of vacancies near the Fermi edge becomes so large that the constraint on occupancy imposed by the Pauli principle is negligible.

In $\mathcal{D}\gg 1$, therefore, if $T/T_v$ is raised gradually, no significant thermal excitations take place initially because $T_v/\bar{T}_v \ll 1$. The isochore stays flat. Once $T$ has reached a certain threshold the Fermi sea is emptied quickly because of its shallowness and the abundance of vacancies close by. The system thus crosses over from a near perfectly degenerate Fermi sea to a nearly ideal MB gas on a very short interval of $T/T_v$ as documented in Fig. 4. In $\mathcal{D}=\infty$ this crossover has sharpened into a phase transition. There is no latent heat involved in that transition and there is no sudden increase in pressure [45].

Note that on the alternative temperature scale $\bar{T}_v$ the emergent crossover between near perfect Fermi sea and almost ideal MB gas is pushed to lower and lower values of $T$ as $\mathcal{D}$ increases, ultimately to $T/\bar{T}_v=0$ for $\mathcal{D}=\infty$. The resultant isochore is then that of the ideal MB gas all the way down.

It is interesting to recall the phase diagram of the ideal BE gas in $\mathcal{D}=\infty$ for comparison. The thermodynamic equation of state inferred from the scaled isochores, isobars, or isotherms as derived, for example, in Ref. [15] has the form

$$pv = \begin{cases} k_B T, & T > T_c \\ 0, & T < T_c, \end{cases} \qquad k_B T_c = 4\pi. \tag{64}$$

As in the FD case there are two phases separated by a transition line at constant $T$. The high-$T$ phase is again an ideal MB gas. The low-$T$ phase is a pure BEC. The transition is of first order and occurs at a higher temperature than in the FD case. Whereas the FD transition disappears in $\mathcal{D}<\infty$, the BE transition persists down to $\mathcal{D}>2$, but is of second order in $\mathcal{D}<\infty$ and occurs along a line in $(p,v,T)$ space that is no longer an isotherm.

### C. Response functions

The three major response functions for a gas of spinless particles are the isochoric heat capacity, $C_v \doteq \mathcal{N}^{-1}(\partial U/\partial T)_v$, the isobaric expansivity, $\alpha_p \doteq v^{-1}(\partial v/\partial T)_p$, and the isothermal compressibility, $\kappa_T \doteq -v^{-1}(\partial v/\partial p)_T$. For the generalized NLS model we must evaluate the expressions

$$\frac{C_v}{k_B} = \left(\frac{\mathcal{D}^2}{4}+\frac{\mathcal{D}}{2}\right)\frac{F_U^{(\mathcal{D})}(z,c_v x)}{F_{\mathcal{N}}^{(\mathcal{D})}(z,c_v x)} - \frac{\mathcal{D}^2}{4}\frac{\dfrac{\partial}{\partial z}F_U^{(\mathcal{D})}(z,c_v x)}{\dfrac{\partial}{\partial z}F_{\mathcal{N}}^{(\mathcal{D})}(z,c_v x)}, \tag{65}$$

$$T_p\alpha_p = \frac{T_p}{T}\left[\left(\frac{\mathcal{D}}{2}+1\right)\frac{F_p^{(\mathcal{D})}(z,c_p y)\dfrac{\partial}{\partial z}F_{\mathcal{N}}^{(\mathcal{D})}(z,c_p y)}{F_{\mathcal{N}}^{(\mathcal{D})}(z,c_p y)\dfrac{\partial}{\partial z}F_p^{(\mathcal{D})}(z,c_p y)} - \frac{\mathcal{D}}{2}\right], \tag{66}$$

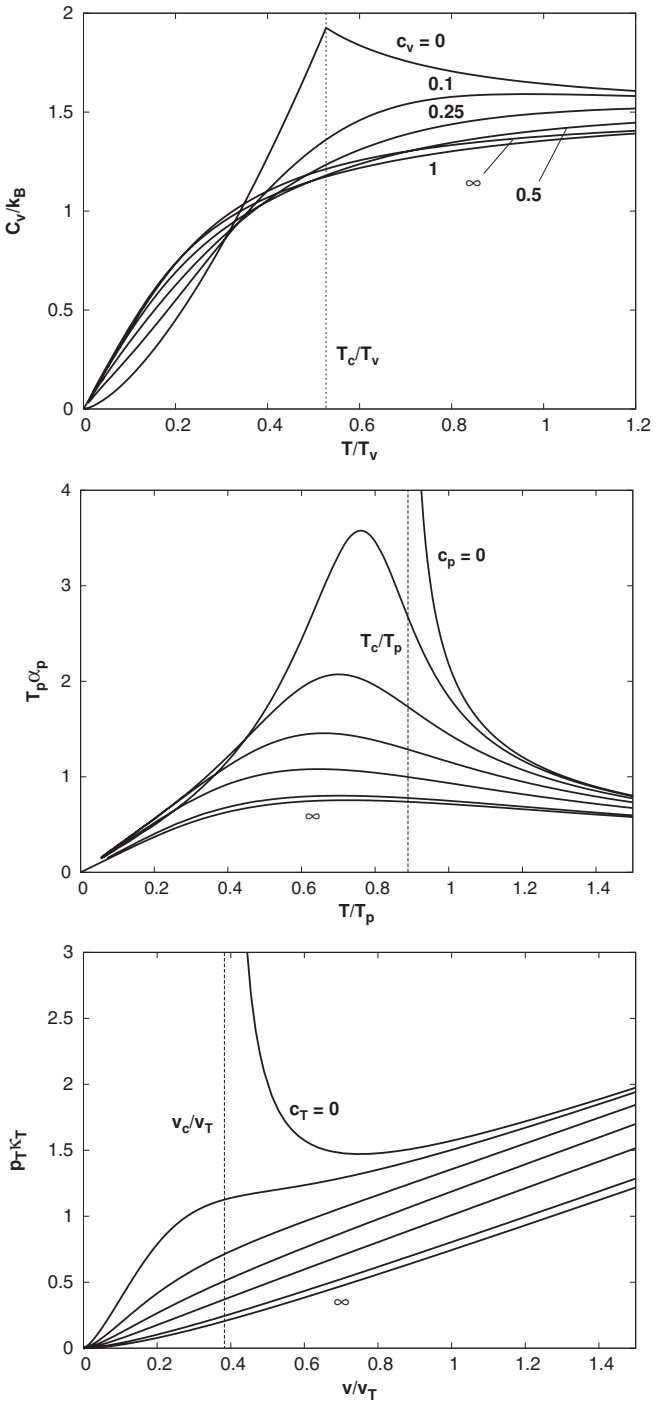


FIG. 5. Isochoric heat capacity, isobaric expansivity, and isothermal compressibility in $D=3$ for $c_{v,p,T}=0,0.1,0.25,0.5,1,3,\infty$. The heat-capacity curves for $c_v=3,\infty$ are unresolved. The dashed lines mark the onset of BEC.

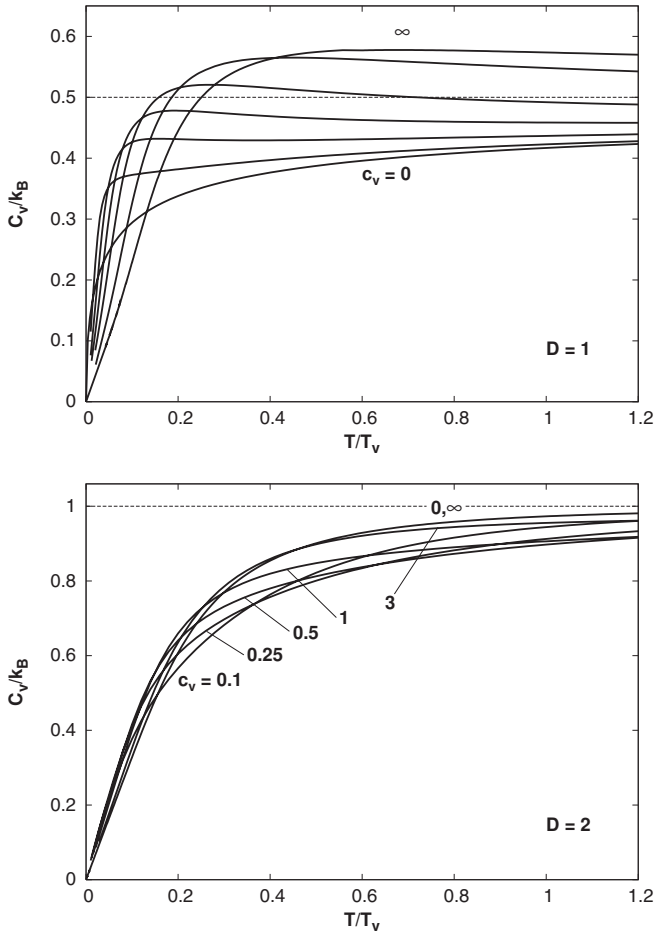


FIG. 6. Isochoric heat capacity in $D=1,2$ for $c_v=0,0.1,0.25,0.5,1,3,\infty$. The dashed lines reflect the high-$T$ asymptotic values $C_v/k_B=\mathcal{D}/2$.

$$p_T\kappa_T = \frac{v}{v_T}\frac{\frac{\partial}{\partial z}F_{\mathcal{N}}^{(\mathcal{D})}(z,c_T)}{\frac{\partial}{\partial z}F_{p}^{(\mathcal{D})}(z,c_T)}, \tag{67}$$

versus the independent variables $T/T_v$, $T/T_p$, and $v/v_T$, respectively, from Eqs. (57)–(59).

In Fig. 5 we show the dependence of each response function on the coupling strength in $\mathcal{D}=3$. The variation of the curves between the BE and FD limits shows some resemblance to that observed in an ideal gas with fractional statistics (generalized CS model) [15]. All three response functions depend only weakly on the statistical interaction at high temperature or low density. The dominant trends there reflect MB behavior, $C_v=(3/2)k_BT$, $\alpha_p=1/T$, $\kappa_T=v/k_BT$. Distinct bosonlike and fermionlike features and crossovers between them emerge at low temperatures and high densities. The exact analytic behavior of the response functions in any $\mathcal{D}$ for the FD and BE limits was described in Ref. [15].

The heat capacity in $\mathcal{D}=3$ for strong coupling is dominated by fermionlike features at all $T$, exhibiting a monotonic descent from the MB asymptote as $T$ is lowered and a linear approach to zero. For weak-coupling the initial increase, the smooth maximum followed by a steep descent is a bosonlike feature. The ultimate linear approach to zero signals the crossover to fermionlike behavior.

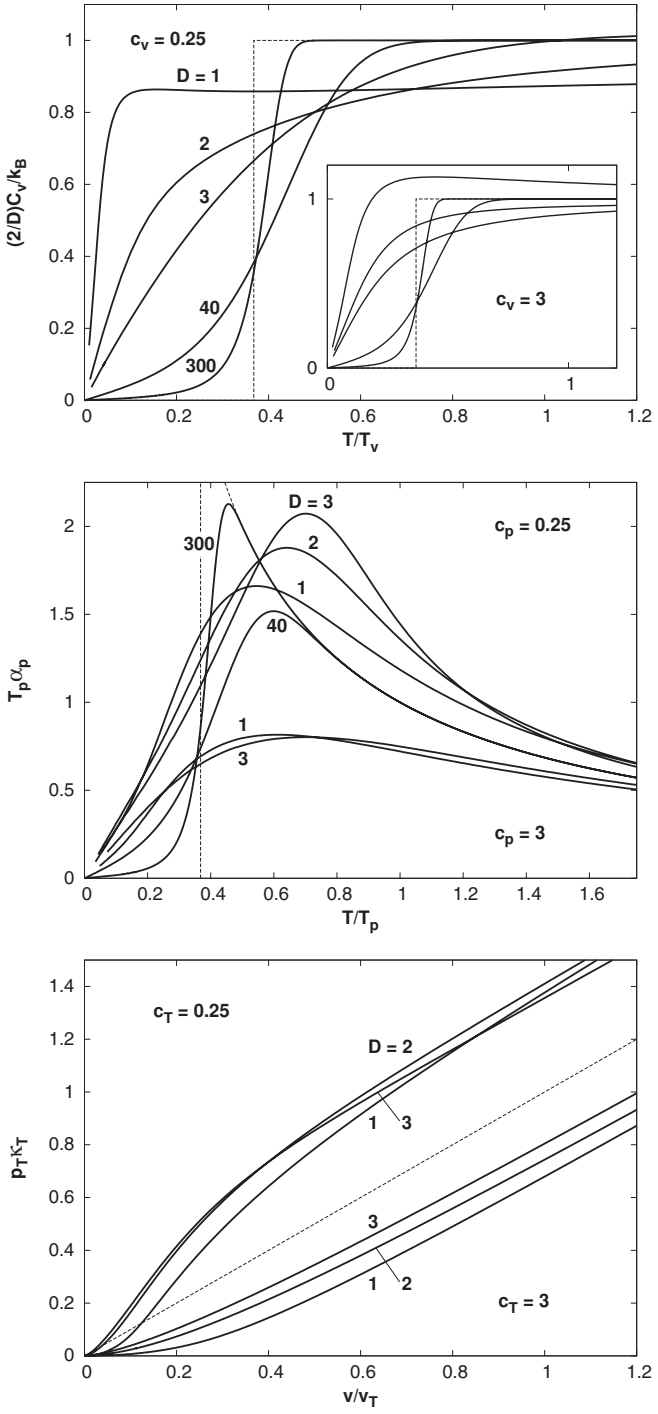


FIG. 7. Isochoric heat capacity (scaled), isobaric expansivity, and isothermal compressibility in $D=1$, 2, 3 for reduced coupling strengths $c_{v,p,T}=0.25$ and $c_{v,p,T}=3$. The dashed lines represent the FD curves for $\mathcal{D}=\infty$. To avoid cluttering we have omitted one expansivity curve.

The expansivity in $\mathcal{D}=3$ depends only weakly on $T$ for strong coupling and approaches zero linearly as $T\to 0$, which is a characteristic fermionlike behavior. For weak coupling the pronounced rise in expansivity is a bosonlike feature.

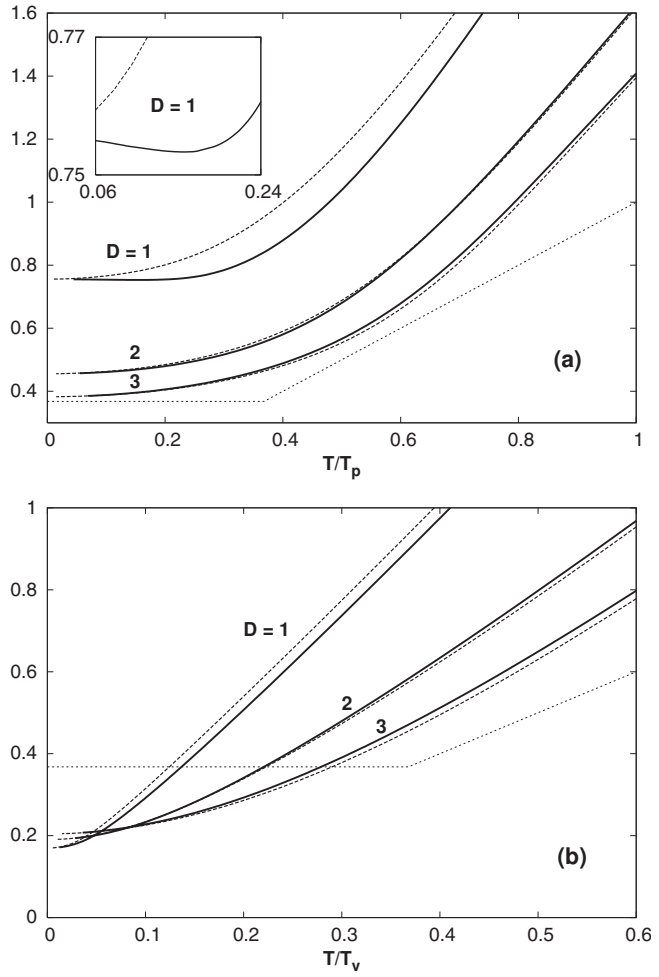


FIG. 8. (a) Main plot: Speed of sound (squared and scaled), $mc^2/k_BT_p$, at constant (average) pressure versus $T/T_p$ in $\mathcal{D}=1,2,3$ (solid lines) and $\mathcal{D}=\infty$ (dotted line). Also shown are scaled isobars, $(1+2/\mathcal{D})(v/v_p)$ versus $T/T_p$ (dashed lines). Inset: Zoomed extract of the $\mathcal{D}=1$ results near the minimum of the speed of sound data. (b) Corresponding data for $mc^2/k_BT_v$ and $(1+2/\mathcal{D})(p/p_v)$ versus $T/T_v$. All data pertain to a weak-coupling situation ($c_{v,p}=0.25$).

However, the repulsive core of the statistical interaction for $\bar{c}>0$, no matter how weak, prevents the expansivity from diverging and forces the fermionlike behavior at low $T$.

Stiff resistance to compression, perhaps the most outstanding fermionlike feature, makes itself manifest with growing strength in the strong-coupling compressibility curves in $\mathcal{D}=3$ as the density is increased. In the weak-coupling curves, on the other hand, we observe trends reminiscent of bosonic behavior at moderate densities. While the BE curve diverges at $v=v_c$, the repulsive core of the statistical interaction prevents the transition from taking place if $\bar{c}>0$. The compressibility curve bends into a smooth maximum or a mere shoulder down to fermionic stiffness.

Similarities to the response functions of an ideal quantum gas with fractional statistics are also manifest in other dimensions $\mathcal{D}$. However, there are two notable exceptions. In Fig. 6 we show the heat capacity for $\mathcal{D}=1,2$ in the same format as the data for $\mathcal{D}=3$ in Fig. 5.

In $\mathcal{D}=2$ the isochoric heat capacity of an ideal quantum gas is well known not to depend on the exclusion statistics [23–27,31,34]. That is no longer the case in the presence of a statistical interaction such as realized in the generalized NLS model. Only the two curves representing the weak-coupling and strong-coupling limits coincide. The curves at intermediate coupling are subject to shifting trends caused by the long-range attractive and short-range repulsive parts of the statistical interaction.

In $\mathcal{D}=1$ the heat capacity curves are monotonically increasing functions near the BE limit and functions with one smooth maximum near the FD limit. Upon variation of the exclusion statistical parameter between the two limits in the quantum ideal gas the appearance of the smooth maximum coincides with a switch in sign of the leading correction to the high-$T$ asymptote [15]. Upon variation of the statistical coupling strength between the same limits in the generalized NLS model, the smooth maximum at low $T$ appears before the approach to the asymptote switches sides from below the asymptote to above it. In consequence there is a range of coupling strengths where the heat capacity has a smooth maximum followed by a smooth minimum.

In Fig. 7 the focus is on the $\mathcal{D}$ dependence of the three response functions at $c_{v,p,T}=0.25$ (weak coupling) and $c_{v,p,T}=3$ (strong coupling). The goal is to gain further insight into how gases with bosonlike, fermionlike, and crossover features in $\mathcal{D}=1,2,3$ evolve into one and the same FD system as $\mathcal{D}\to\infty$ with an emergent singularity at $T/T_v=T/T_p=e^{-1}$ in isochoric and isobaric processes.

For the scaled heat capacity we show weak-coupling results in the main plot and strong-coupling results in the inset. The dependence on coupling strength of the results in $\mathcal{D}=1,2,3$ is conspicuous but becomes imperceptibly small for $\mathcal{D}\gtrsim 20$. The universal FD result for $\mathcal{D}=\infty$ (dashed line) is a simple step function,

$$\lim_{\mathcal{D}\to\infty}\frac{C_v}{(\mathcal{D}/2)k_B}=\Theta(T-T_c),\quad T_c/T_v=e^{-1}. \tag{68}$$

The decrease in initial slope with increasing $\mathcal{D}$ is clearly visible in the curves for $\mathcal{D}=1,2,3$ but overall convergence toward the step function is slow. The scaled heat capacity of the ideal BE gas in $\mathcal{D}=\infty$ also consists of two terms, one being a step function as in Eq. (68) but with $T_c/T_v=1$ and the other being a $\delta$ function representing the latent heat [15].

For the isobaric expansivity the weak-coupling and strong-coupling curves are shown in the same plot. There is very little variation between $\mathcal{D}=1$ and $\mathcal{D}=3$ for the strong-coupling case ($c_p=3$). Somewhat larger and more systematic variation occurs in the weak-coupling case ($c_p=0.25$). The universal FD result for $\mathcal{D}=\infty$ (shown dashed) is

$$T_p\kappa_p=\frac{T_p}{T}\Theta(T-T_c),\quad T_c/T_p=e^{-1}. \tag{69}$$

Convergence is slow, but evident in the curves for $\mathcal{D}=40,300$. Comparing the result (69) for the ideal FD gas with

that of the ideal BE gas, both in $\mathcal{D}=\infty$, we find that the latter also has the form (69) at $T>T_c$ but with $T_c/T_p=1$. The expansivity of the FD gas is zero at $T<T_c$; in the BE gas it is undefined [15].

For the isothermal compressibility the universal FD line for $\mathcal{D}=\infty$ (dashed line),

$$p_T\kappa_T = \frac{v}{v_T}, \tag{70}$$

is indistinguishable from the MB result. The weak-coupling and strong-coupling curves are located on opposite sides of that line. Convergence is apparent in the curves for $\mathcal{D}=1,2,3$ in the strong-coupling case ($c_T=3$) but not in the weak-coupling case ($c_T=0.25$). The isothermal compressibility of ideal BE gas is also described by the result (70) but only for $v/v_T>v_c/v_T=1$. At $v/v_T<1$ the bosonic result is infinite [15].

### D. Speed of sound

The speed of sound as inferred from $c=(\rho\kappa_S)^{-1/2}$, where $\rho=m/v$ is the mass density and $\kappa_S$ is the adiabatic compressibility, can be brought into the form [46]

$$\frac{mc^2}{k_BT} = \frac{(v/v_T)}{(p_T\kappa_T)}\left[1+\frac{(T/T_p)^2(v/v_T)(T_p\alpha_p)^2}{(p_T\kappa_T)(C_v/k_B)}\right], \tag{71}$$

which only involves dimensionless quantities previously determined in terms of the NLS functions,

$$\frac{mc^2}{k_BT} = \frac{\frac{\partial}{\partial z}F_p^{(\mathcal{D})}(z,\bar{c})}{\frac{\partial}{\partial z}F_{\mathcal{N}}^{(\mathcal{D})}(z,\bar{c})}\left\{1+\frac{2}{\mathcal{D}}\frac{\frac{\partial}{\partial z}F_p^{(\mathcal{D})}(z,\bar{c})}{\frac{\partial}{\partial z}F_U^{(\mathcal{D})}(z,\bar{c})}\frac{\left[\left(\frac{\mathcal{D}}{2}+1\right)\frac{F_p^{(\mathcal{D})}(z,\bar{c})\frac{\partial}{\partial z}F_{\mathcal{N}}^{(\mathcal{D})}(z,\bar{c})}{F_{\mathcal{N}}^{(\mathcal{D})}(z,\bar{c})\frac{\partial}{\partial z}F_p^{(\mathcal{D})}(z,\bar{c})}-\frac{\mathcal{D}}{2}\right]^2}{\left[\left(\frac{\mathcal{D}}{2}+1\right)\frac{F_U^{(\mathcal{D})}(z,\bar{c})\frac{\partial}{\partial z}F_{\mathcal{N}}^{(\mathcal{D})}(z,\bar{c})}{F_{\mathcal{N}}^{(\mathcal{D})}(z,\bar{c})\frac{\partial}{\partial z}F_U^{(\mathcal{D})}(z,\bar{c})}-\frac{\mathcal{D}}{2}\right]}\right\}. \tag{72}$$

Here $\bar{c}$ must be replaced by $c_T$, $c_v x$, or $c_p y$ depending on whether we are considering an isothermal, isochoric, or isobaric process, respectively. In Fig. 8 we present data for the $T$ dependence of the speed of sound of a weak-coupling system under isobaric and isochoric conditions.

It is well known that in ideal gases the curves for $mc^2/k_BT$ differ from those of the isobars or isochores only by a multiplicative factor $(1+2/\mathcal{D})$. We have seen that this relation still holds in the presence of fractional statistics [15]. The data shown here for the generalized NLS model demonstrate that no such relation holds any longer in the presence of a statistical interaction that is not reducible to a simple exclusion principle.

The deviations appear to be strongest in $\mathcal{D}=1$. All deviations are expected to fade away in the limit $\mathcal{D}\to\infty$ when ideal gas behavior is restored as explained in Sec. IV B. Particularly noteworthy is the observation that the $T$ dependence of the speed of sound in $\mathcal{D}=1$ at constant (average) pressure undergoes a minimum as highlighted in the inset. No such minimum exists in the isobar.

We attribute this effect to the crossover between bosonlike features at high $T$ and fermionlike features at low $T$. The general trend, realized in ideal gases is that the speed of sound decreases monotonically upon cooling. Superimposed on this is another trend that signals softness when bosonlike features are predominant and stiffness when fermionlike features are predominant.

For stronger coupling (e.g., $c_{v,p}=3$) the deviations of the speed-of-sound data from the scaled isobar or isochore are of a similar kind and size. We have detected no minimum at $T>0$ in these data. If such a minimum exists at all it must occur at very low $T$, out of reach of our numerical analysis.

## V. CONCLUSION

The exact thermodynamic analysis of the generalized NLS model, a quantum gas in $\mathcal{D}$ dimensions with a statistical two-body interaction, has yielded significant deviations from characteristic ideal quantum gas behavior in several respects.

For given coupling strength $0<c<\infty$ (i) the average level occupancy $\langle n(k)\rangle$ is no longer a unique function of $(k^2-\mu)/k_BT$ and independent of $\mathcal{D}$; (ii) the quantities $p\lambda_T^{\mathcal{D}}/k_BT$, $\mathcal{N}\lambda_T^{\mathcal{D}}/V$, and $(U\lambda_T^{\mathcal{D}}/V)/(k_BT\mathcal{D}/2)$ are no longer unique functions of the fugacity $z$; and (iii) the two quantities $p\lambda_T^{\mathcal{D}}/k_BT$ and $(U\lambda_T^{\mathcal{D}}/V)/(k_BT\mathcal{D}/2)$ are no longer identical.

Among the consequences are (i) that the $T$ dependence of the internal energy is no longer of the same shape as the

isochore; (ii) that the quantity $pV/\mathcal{N}k_BT$ is no longer a function of $z$ alone in given $\mathcal{D}$; (iii) that there is no longer anysimple relation between the speed of sound and the isochore or isobar.

In any finite $\mathcal{D}$ the statistical interaction of the generalized NLS model smoothly interpolates between an ideal BE gas in the weak-coupling limit ($c=0$) and an ideal FD gas in the strong-coupling limit ($c=\infty$). In the limit $\mathcal{D}\to\infty$ the system behaves like an ideal BE gas for $c=0$ and like an ideal FD gas for $c>0$. In $\mathcal{D}=\infty$ both quantum gases feature a phase transition at $T_c>0$ along isochores or isobars. The transition is of first order in the BE case and of second order in the FD case.

## ACKNOWLEDGMENTS

Financial support from the DFG Schwerpunkt *Kollektive Quantenzustände in elektronischen 1D Übergangsmetallverbindungen* (for M.K.) is gratefully acknowledged. We have greatly benefited from discussions with Professor A. E. Meyerovich.

[1] C. J. Pethick and H. Smith, *Bose-Einstein Condensation in Dilute Gases* (Cambridge University Press, Cambridge, England, 2002).
[2] L. Pitaesvskii and S. Stringari, *Bose-Einstein Condensation* (Oxford University Press, New York, 2003).
[3] M. Greiner, I. Bloch, O. Mandel, T. W. Hänsch, and T. Esslinger, Phys. Rev. Lett. **87**, 160405 (2001).
[4] A. Görlitz *et al.*, Phys. Rev. Lett. **87**,130402 (2001).
[5] F. Schreck, L. Khaykovich, K. L. Corwin, G. Ferrari, T. Bourdel, J. Cubizolles, and C. Salomon, Phys. Rev. Lett. **87**, 080403 (2001).
[6] D. S. Petrov, D. M. Gangardt, and G. V. Shlyapnikov, J. Phys. IV **116**, 5 (2004).
[7] Y.-S. Wu, Phys. Rev. Lett. **73**, 922 (1994).
[8] Y. S. Wu, in *New Development on Integrable Systems and Long-Ranged Interaction Models*, edited by M. I. Ge and Y. S. Wu (World Scientific, Singapore, 1995), p. 159; Y. S. Wu, in *Proceedings of the 20th International Conference on Group Theoretical Methods in Physics*, edited by A. Arima, T. Eguchi, and N. Nakanishi (World Scientific, Singapore, 1995), p. 94.
[9] F. D. M. Haldane, Phys. Rev. Lett. **67**, 937 (1991).
[10] F. D. M. Haldane, Phys. Rev. Lett. **66**, 1529 (1991).
[11] F. D. M. Haldane, in *Correlation Effects in Low-Dimensional Electron Systems*, edited by A. Okiji and N. Kawakami (Springer-Verlag, Heidelberg, 1994).
[12] D. Bernard and Y.-S. Wu, *New Developments on Integrable Systems and Long-Ranged Interaction Models* (World Scientific, Singapore, 1994).
[13] M. Arikawa, M. Karbach, G. Müller, and K. Wiele, J. Phys. A **39**, 10623 (2006).
[14] An effort with similar goals but different strategy was reported by B. Sutherland, Phys. Rev. B **56**, 4422 (1997).
[15] G. G. Potter, G. Müller, and M. Karbach, Phys. Rev. E **75**, 061120 (2007).
[16] F. Calogero, J. Math. Phys. **12**, 419 (1971).
[17] B. Sutherland, Phys. Rev. A **4**, 2019 (1971).
[18] B. Sutherland, Phys. Rev. A **5**, 1372 (1972).
[19] S. B. Isakov, Int. J. Mod. Phys. A **9**, 2563 (1994).
[20] S. B. Isakov, D. P. Arovas, J. Myrheim, and A. P. Polychronakos, Phys. Lett. A **212**, 299 (1996).
[21] G. S. Joyce, S. Sarkar, J. Spalek, and K. Byczuk, Phys. Rev. B **53**, 990 (1996).
[22] M. V. N. Murthy and R. Shankar, Phys. Rev. B **60**, 6517 (1999).
[23] R. M. May, Phys. Rev. **135**, A1515 (1964).
[24] T. Aoyama, Eur. Phys. J. B **20**, 123 (2001).
[25] M. H. Lee, Phys. Rev. E **55**, 1518 (1997).
[26] A. Swarup and B. Cowan, J. Low Temp. Phys. **134**, 881 (2004).
[27] D.-V. Anghel, J. Phys. A **35**, 7255 (2002).
[28] C. Nayak and F. Wilczek, Phys. Rev. Lett. **73**, 2740 (1994).
[29] K. Iguchi, Phys. Rev. Lett. **78**, 3233 (1997).
[30] K. Iguchi, Mod. Phys. Lett. B **11**, 765 (1997).
[31] K. Iguchi, Int. J. Mod. Phys. B **11**, 3551 (1997).
[32] K. Iguchi and K. Aomoto, Int. J. Mod. Phys. B **14**, 485 (2000).
[33] M. V. Medvedev, Phys. Rev. Lett. **78**, 4147 (1997).
[34] S. Viefers, F. Ravndal, and T. Haugset, Am. J. Phys. **63**, 369 (1995).
[35] E. Lieb and W. Liniger, Phys. Rev. **130**, 1605 (1963).
[36] E. H. Lieb, Phys. Rev. **130**, 1616 (1963).
[37] C. N. Yang and C. P. Yang, J. Math. Phys. **10**, 1115 (1969).
[38] C. P. Yang, Phys. Rev. A **2**, 154 (1970).
[39] V. E. Korepin, N. M. Bogoliubov, and A. G. Izergin, *Quantum Inverse Scattering Method and Correlation Functions* (Cambridge University Press, Cambridge, England, 1993).
[40] M. Takahashi, *Thermodynamics of One-Dimensional Solvable Models* (Cambridge University Press, Cambridge, England, 1999).
[41] B. Sutherland, *Beautiful Models: 70 Years of Exactly Solved Quantum Many-Body Problems* (World Scientific, Singapore, 2004).
[42] The same argument applies to the case $\bar{c}=0$ but only for $z\leqslant 1$. Indeed we have $f_\infty(z)=g_\infty(z)=z$ for $0\leqslant z\leqslant 1$.
[43] R. K. Pathria, *Statistical Mechanics* (Pergamon Press, Oxford, 1972).
[44] In $\mathcal{D}=\infty$, $pv$ and $k_BT$ become dimensionless under the convention $\hbar^2/2m=1$ used here.
[45] The scaled entropy $S/\mathcal{N}\mathcal{D}$ rises from zero at $T\geqslant T_c$ with finite slope.
[46] For consistency, we must use reference values $T_v$, $T_p$, and $v_T$ derived from the first expression (37) for $\lambda_T$ in this context.